Blobby Cross-Field Plasma Transport In Tokamak Edge

S. I. Krasheninnikov 1,6), A. Yu. Pigarov 1,6), S. A. Galkin 1), G. Q. Yu 1),
D. A. D Ippolito 2), J. R. Myra 2), D. R. McCarthy 3), W. M. Nevins 4), T. D. Rognlien 4),
X. Q. Xu 4), J. A. Boedo 1), D. L. Rudakov 1), M. J. Schaffer 5),
W. P. West 5), and D. G. Whyte 1)

1) University of California San Diego, La Jolla, California, USA
2) Lodestar Research Corporation, Boulder, Colorado, USA
3) Southeastern Louisiana University, Hammond, Louisiana, USA
4) Lawrence Livermore National Laboratory, Livermore, California, USA
5) General Atomics, San Diego California, USA
6) Kurchatov Institute of Atomic Energy, Moscow, Russia

e-mail contact of main author: skrash@mae.ucsd.edu

Abstract. Recent studies suggest rather fast radial plasma transport in tokamak scrape off layer (SOL). Moreover, it seems that this transport has not diffusive but convective-like features. One of the plausible mechanisms of this fast convective SOL plasma transport can be associated with plasma blobs . Such blobs have been observed in many experiments. Here we present the results of our investigations of different aspects of blobby non-diffusive transport in the SOL ranging from the simplified analytic theory of individual blob propagation, to the 2D and 3D modeling of blobs with turbulence codes, and, finally, the macroscopic modeling of edge plasma transport in DIII-D tokamak.

Introduction. Recent analysis of experimental data from various tokamaks suggests that plasma coming into the SOL from the bulk region can recycle at the wall of the main chamber [1-3], rather than flowing into the divertor and recycling there as the conventional picture of edge plasma flows would suggest. This analysis implies rather fast radial plasma transport in the SOL of main chamber. Moreover, in order to be compatible with experimental observations, radial transport should be convective rather than diffusive [1].

One of the possible mechanisms of fast convective plasma transport in the SOL can be associated with plasma blobs [4] observed in many experiments (e. g. [5-11]). These are coherent structures extended along the magnetic field lines with density of the order of the separatrix density which is much higher than the ambient plasma density in the far SOL. The origin of these blobs in the SOL can be rather strong plasma turbulence in the separatrix region causing plasma blobs to peel off from the bulk plasma.

In this report we present the results of our studies of different aspects of fast non-diffusive plasma transport in the SOL: the simplified analytic theory of individual blob propagation, the 2D and 3D modeling of the blobs with turbulence codes, and, finally, the macroscopic transport modeling of the edge plasma transport in tokamaks.

Analytic Theory. The ∇B drift of charged particles in a tokamak magnetic field results in plasma polarization and, correspondingly, in the **E**×**B** plasma flow. The **E**×**B** flow becomes rather strong in the SOL due to the effective sheath resistivity [13] when the plasma contacts the divertor target. For $T_i = 0$ and constant T_e, we have the simplest 2D equations for the SOL plasma dynamics accounting for these effects (e. g. [14, 4])

$$\rho_s^2 \nabla_\perp \cdot \left(n d_t \nabla_\perp \phi \right) + \rho_s (2C_s / R) \partial_y n = (2C_s / L) n \phi , \qquad (1a)$$

$$d_t n = -2C_s \left(n - n_{ion}(x) \right) / L , \qquad (1b)$$

where n is the plasma density, $\phi = e\varphi / T_e$, e is the electron charge, φ is the electrostatic potential, the axis y (x) is perpendicular (parallel) to ∇B and , $C_s = \sqrt{T_e / M}$, $\rho_s = C_s / \omega_{Bi}$, M and ω_{Bi} are the ion mass and gyrofrequency, $d_t(...) = \partial_t(...) + \mathbf{V}_{E\times B} \cdot \nabla(...)$, $\mathbf{V}_{E\times B} = C_s \rho_s (\mathbf{b} \times \nabla\varphi)$, $\mathbf{b} = \mathbf{B}/B$, R is the tokamak effective major radius, L is the connection length, and $n_{ion}(x)$ describes the plasma ionization source. In the case where the leakage of plasma to the divertor is small, we find blobby solutions of (1) in the form of a traveling wave [4]

$$n(t,x,y) = n_b(x - V_b t, y) \equiv n_b^{(x)}(x - V_b t) \times \exp\left(-(y/\delta_b)^2\right), \qquad (2a)$$

$$\left(\mathbf{V}_{E\times B}\right)_x = -C_s (L/2R) \rho_s^2 \left(\partial^2 \ln(n) / \partial y^2\right), \qquad (2b)$$

where $n_b^{(x)}(x)$ is an arbitrary function, δ_b is the blob poloidal size scale, $\mathbf{V}_{E\times B} = \mathbf{V}_b \equiv \mathbf{e}_x V_b$, and V_b is the blob velocity which equals to

$$V_b = C_s \left(\rho_s / \delta_b\right)^2 (L/R). \qquad (3)$$

Deriving expressions (2), (3) we neglected the leakage of plasma blobs along the magnetic field line to the targets, which implies that our estimates for the importance of cross-field plasma motion should satisfy $\tau_{||} \sim L/C_s > \tau_\perp > \delta_b / V_b$ (we assume that the cross-field scale of blob $\sim \delta_b$). It results in the following restrictions for the blob s scale and velocity

$$V_b > V_{min} \sim C_s \left(\rho_s / R\right)^{2/3} (\pi q)^{-1/3}, \qquad \delta_b < \delta_{max} \sim \left\{(\pi q)^2 R \rho_s^2\right\}^{1/3}. \qquad (4)$$

In Eq. (4) we take $L \sim \pi q R$, where q is the safety factor.

Solution (2) assumes no background plasma density ($n_{y\to\pm\infty} \to 0$). In practice, background plasma density, n_0, superimposed on blob density (2a) results in the shear of plasma velocity, $\mathbf{V}_{E\times B}$, see (2b). Therefore, for $n_b \tilde{>} n_0$, the blobby solution (2) still holds for the case where the impact of the vorticity term in Eq. (1a), which can cause Kelvin-Helmholtz instability, can be neglected. It implies $(\rho_s/\delta_b)^2 V_b / \delta_b < C_s / L$, and causes the following restrictions for a blob parameters

$$V_b < V_{max} \sim C_s \left(\rho_s / R\right)^{2/5} (\pi q)^{-1/5}, \qquad \delta_b > \delta_{min} \sim \left\{(\pi q)^2 R \rho_s^4\right\}^{1/5}. \qquad (5)$$

In Eq. (5) we take $L \sim \pi q R$. For C-Mod/DIII-D edge plasma parameters, we estimate the possible ranges of blob velocity and size [15]:

$$V_{min} \sim 150 \text{ m/s} < V_b < V_{max} \sim 5000 \text{ m/s}, \quad \delta_{min} \sim 0.5 \text{ cm} < \delta_b < \delta_{max} \sim 3 \text{ cm}. \quad (6)$$

We notice that the difference in estimates (6) for C-Mod and DIII-D conditions is rather small even though the C-Mod and DIII-D parameters differ significantly.

Taking into account the leakage to the targets, blobs can propagate radially for the distance $\Delta_b \sim V_b \tau_{||} \sim V_b L / C_s < V_{max} L / C_s$. As a result we find the maximum radial distance, Δ_{max}, that the blobs can propagate before plasma leaks to the targets along the magnetic field lines,

$$\Delta_b < \Delta_{max} \sim \left\{\rho_s^2 R^3 (\pi q)^4\right\}^{1/5} \sim 30\ \text{cm}. \qquad (7)$$

Rather strong dependence of blob radial velocity on blob s radial δ_b scale, $V_b \propto \delta_b^{-2}$, implies that the average radial transport (averaged over an ensemble of blobs) will be determined by the blob perpendicular scale distribution, $f_b(\delta_b)$. For example, assuming a power law distribution, $f_b(\delta_b) \propto \delta_b^{-p}$ (where p is an adjustable parameter), we find (see Fig. 1) that radial profiles of both averaged plasma density and radial flux are sensitive to the blob size distribution [16]. For $p = 1$, large blobs dominate the ensemble average and the profiles decay rapidly along normalized radial coordinate x_n; for large p, small blobs dominate so that the profiles flatten. For a fixed parallel transit time to the wall $\tau_{||} \sim L/C_s$, the small, fast blobs penetrate farther into the SOL than the large, slow blobs, yielding a larger convective contribution to the transport in far SOL. We note that both the flux and density profiles which follow from our model are in a reasonable agreement with recent experimental data [7].

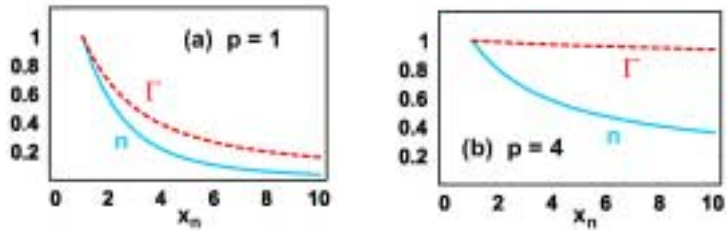

Fig. 1. Averaged plasma density (dashed line) and radial flux (solid line) profiles as a functions of the normalized radial coordinate x_n for (a) p=1 and (b) p=4.

It is useful to estimate how many blobs are needed to establish a total plasma particle flux to the wall $\sim 10^{21} \div 10^{22}\ s^{-1}$ as is seen in the tokamak experiments. We estimate the number of particle in one blob, $N_b \sim n_b L \delta_b^2$,

$$N_b < N_{max} = n_b L \delta_{max}^2 \sim n_b R^3 \left((\pi q)^7 (\rho_s/R)^4\right)^{1/3}. \qquad (8)$$

For C-Mod/DIII-D edge plasma parameters we find $N_{max} \sim 10^{17}$. Therefore, to establish total plasma particle flux $\sim 10^{21} \div 10^{22}\ s^{-1}$ with $N_b \sim 10^{16} < N_{max}$ it is sufficient to have blob formation rate $F_b = 10^{5\div 6}\ s^{-1}$ (as seen in DIII-D). If the poloidal length along the separatrix where blob transport occurs is, $s \sim 50\,\text{cm}$, and blob scale $\delta_b \sim 1$ cm, the rate F_b corresponds to the frequency of plasma turbulent oscillations producing blobs, ω_b, estimated as $\omega_b \sim F_b \times (\delta_b / s)$ and gives $\omega_b \sim 10^{3\div 4}\ s^{-1}$, which is below the drift wave frequency range. This shows that blob formation and peeling off from the main plasma are rather rare events.

The overall physical picture of blobby transport in the SOL plasma presented here as well as the estimates of blob typical spatial scale and radial velocity (6) seems to be consistent with experimental observations on C-Mod, DIII-D, and NSTX [6-8, 12].

2D and 3D Numerical Modeling of Coherent Structures Dynamics in the SOL. The main focus of this study was on the dynamics of individual coherent structures, blobs and dips (hills and vallies in plasma density), in the SOL plasma. The mechanisms of how the blobs are peeled off from bulk plasma and penetrate into the SOL or how dips are

formed will be reported elsewhere. Here we just seed such structures in constant density SOL plasma and then follow their evolution. In 2D modeling we use Eq. (1), with diffusion added to the equation (1b), as a governing equations describing dynamics of coherent structures. The diffusion coefficient we used was small and did not greatly affect the overall picture of blob dynamics while it helped the stability of our numerical schemes. To be relevant to current experiments, in our 2D modeling we take the following parameters: $R = 175\,\mathrm{cm}$, $L = 4\times10^{3}\,\mathrm{cm}$, $T_e \sim 50\,\mathrm{eV}$, and $\rho_s = 6\times10^{-2}\,\mathrm{cm}$.

First we start with a study of the blob s dynamics. We take a constant plasma density background, n_0, with the magnitude much smaller than plasma density in the blob n_b and then vary the spatial scale of the blob. We find that in agreement with our analytic consideration relatively large blobs ($\delta_b > \delta_{min}$) propagate radially to large distances (~ 10 cm) as a coherent structures. Somewhat similar behavior of large blobs were reported recently in [17]. In Fig. 2 we show the evolution of density contours of a large blob with initial spatial scales 1.2 cm. Radial velocity of the blob in Fig. 2 is about $7\,\mathrm{km/s}$.

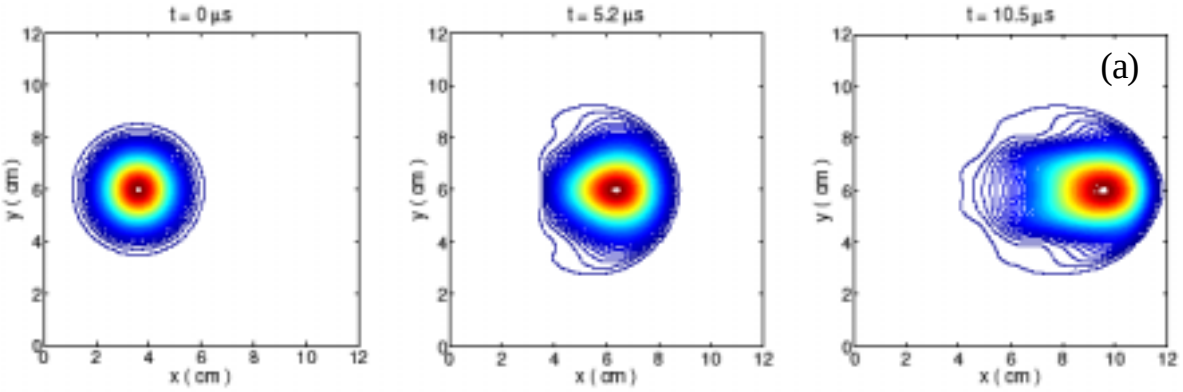

Fig. 2. Evolution of density contours for a blob with initial spatial scale $\delta_b = 1.2$ cm.

Smaller blobs ($\delta_b \le \delta_{min}$) quickly cease to exist as initially coherent structures. Instead, mushroom-like and then even more complex structures with rich dynamics emerge. We find, see Fig. 3, that jet-like streams with a spatial scale smaller than the initial blob are ejected from these structures and propagate radially to relatively large distances before they stop.

Comparing the dependence of blob velocity on spatial scale found from numerical modeling with the scaling (3), we find that the velocities of large blobs follow expression (3) pretty well, while smaller blobs ($\delta_b < \delta_{min}$) are much slower than expected from (3).

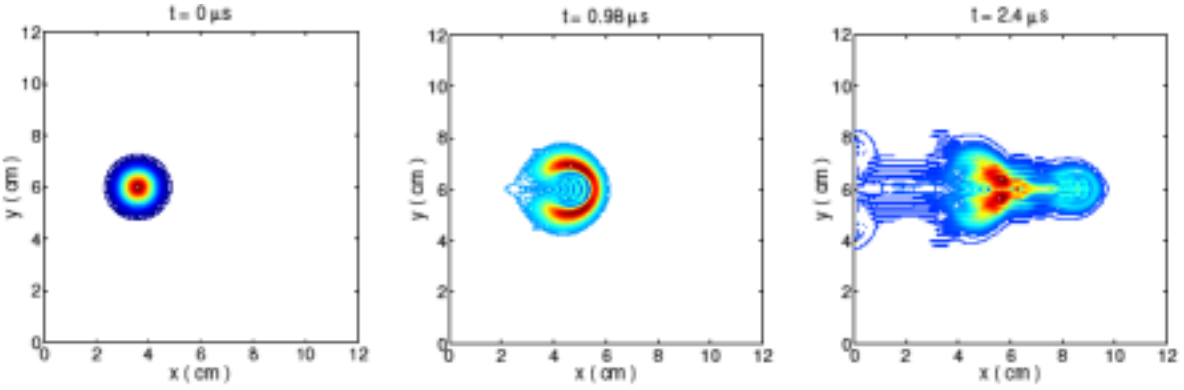

Fig. 3. Evolution of density contours for a blob with initial spatial scale $\delta_b = 0.6$ cm.

Next we study the evolution of the dips of plasma density in the SOL plasmas. While the ∇B polarization of the blobs causes their ballistic motion to the wall, the ∇B polarization of the dips will cause dip to move toward the core. Such features of dip motion are observed in our 2D modeling [18] and have been seen experimentally near the separatrix [7, 19], where dip diagnostic is easier. Ballistic motion of dips can explain the penetration of impurity from the wall to the core often seen in experiments. Indeed, neutral impurity atoms/molecules, being sputtered from the wall, fly to the plasma and, finally, are ionized at some distance from the wall. Neutral impurities that are ionized within the blobs will be immediately carried away to the wall by the blob motion and will not contribute to core plasma contamination. But impurities that are ionized within the dips can be convectively carried towards the core.

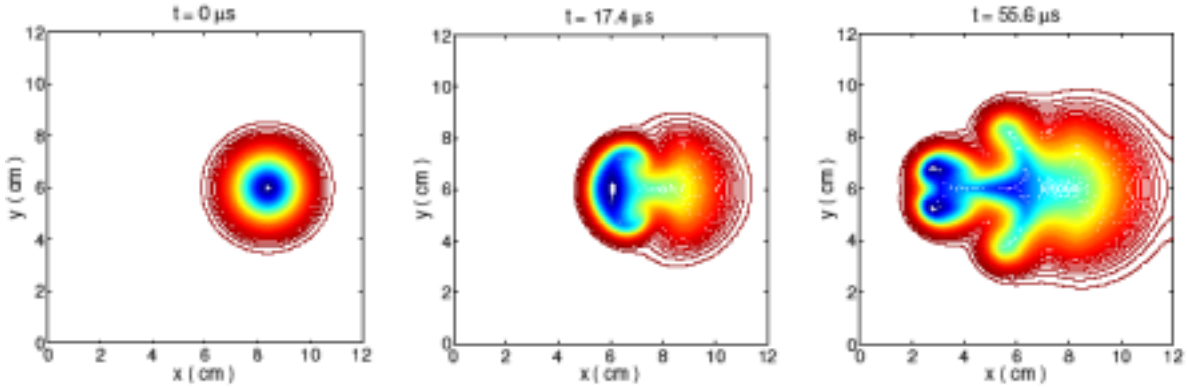

Fig. 4. Evolution of density contours for a dip with $n_d/n_0 = 0.5$ *and* $\delta_d = 1.2$ cm.

However, the dynamics of an individual dip can significantly differ from that of a blob. The reason is the difference in the magnitudes between the blob and dip plasma density excursions from the background. The magnitude of the blob density, n_b, is not restricted and can be much larger than background plasma density n_0. The magnitude of the dip density, n_d, is restricted, $n = n_0 - n_d > 0$, therefore $n_d < n_0$. Then, recalling expression (2b), we conclude that the impact of the velocity shear and, therefore, vorticity effects, on dip dynamics may be rather strong. We studied the dynamics of dip plasma motion numerically and found that indeed vorticity effects play a very important role in dip dynamics. Vorticity slows down the inward dip propagation and even breaks the dips into pieces. We also found jet-like streams that, similar to those found for the case of small-scale blob evolution, propagate radially for relatively large distances (see Fig. 4). More work is needed to assess the impact of dip dynamics on impurity transport in the SOL.

We also apply the 3D turbulence code BOUT [20] to study the evolution of seeded blobs in the SOL of circular tokamak with toroidal limiter at the bottom of the first wall. We take just slightly varying background plasma density and temperature ($T \sim 15\,eV$) profiles and the amplitude of plasma density in the blob about two times larger then background.

In Fig. 5a we show poloidal projection of plasma density averaged over toroidal angle. Due to finite resistivity effects the large radius side of the blob propagates outward while the small radius side stays almost at the same position. At the same time the outer side of the blob moves poloidally due to radial electric field effects (radial electric field is due to radial inhomogeneity of the temperature). As a result, plasma density along a fixed radial chord at the outer side decreases with time (see Fig. 5b). Notice that the radial velocity of the blob ($\sim 6\,km/s$) inferred from the BOUT 3D modeling is, in general, consistent with both analytic estimates and 2D results.

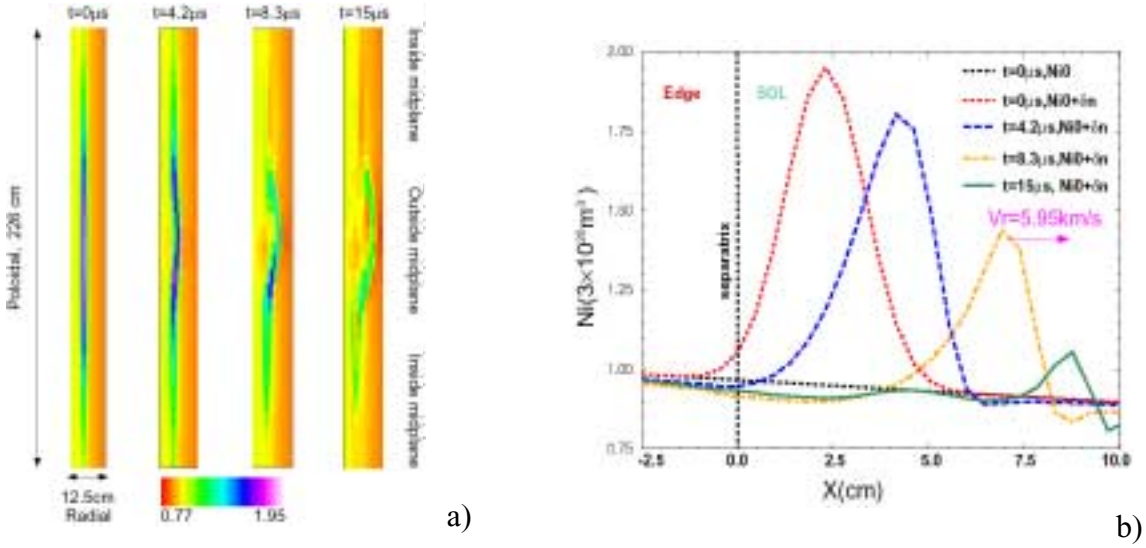

Fig. 5. 3D evolution of density blob in edge plasma found from BOUT modeling.

Macroscopic Modeling of the Edge Plasma Transport in Tokamaks. An important question is then how these microscopic phenomena we discussed before are reflected in the macroscopic plasma transport. To find it we implement into the 2D edge transport code UEDGE [21] a plasma transport model which includes both diffusive and outward convective terms for cross-field plasma particle flux, $j_r(r,\vartheta)$, [22]

$$j_r(r,\vartheta) = -D\frac{\partial n}{\partial r} + V_{conv}(r,\vartheta)n, \qquad (8)$$

where r is minor radius and ϑ is the poloidal angle. In our model V_{conv} was always positive. To mimic the ballooning feature of blobby transport the magnitude of $V_{conv}(r,\vartheta)$ at the outer side of the torus was made significantly larger then that at the inner side. To describe the effects of blobby transport on the far SOL plasma parameters, we took $V_{conv}(r,\vartheta)$ to be rather small close to separatrix and increasing with increasing r. We benchmark this model against DIII-D discharges. The results of our modeling confirm the crucial importance of convective transport for the edge plasma. We demonstrate that convective transport has equally important effects on the averaged plasma characteristics in both the main chamber and the divertor. Modeling of DIII-D discharges with mixed anomalous diffusion/convection model for radial plasma transport [22, 23] allows us successfully match experimental data which could not be matched otherwise.

As an example, in Fig. 6 we show D_α intensity along different viewing chords in L mode discharge (#105500) on DIII-D tokamak [22]. Recall that for tokamak conditions D_α represents the plasma ionization source and, therefore, indicates the return of lost plasma particles. Inclusion of convection leads to strongly enhanced recycling of plasma on the wall of main chamber and, therefore, D_α signal caused by plasma-neutral interactions. As a result we are able to fit the outermost chords of D_α diagnostics which is not possible to do without invoking convective plasma transport (see Fig. 6).

We model a series of DIII-D L-mode discharges having different averaged plasma densities $\langle n_e \rangle$ at the same NBI input [23]. We find that to fit experimental data the magnitude of V_{conv} should increase with increasing $\langle n_e \rangle$. In Fig. 7 we show comparison of experimental data with the results of our modeling for different $\langle n_e \rangle$. The observed dependence of V_{conv} on $\langle n_e \rangle$ is an indication of an overall increase of plasma transport

with increasing plasma density. In Fig. 7 one also sees a nonlinear increase of cross-field transport to the wall. Nonlinearity is seen from a cubic fit to $\langle n_e \rangle$ dependence of both D_α signal and neutral gas pressure, P_N, measured and simulated at mid plane. Notice that D_α signal and P_N are the measures of neutral influx into core plasma which balances the plasma outflux. Fig. 7 also shows that the percentage of core fueling due to main chamber recycling ($\Gamma_{main}/\Gamma_{total}$) increases with increasing $\langle n_e \rangle$. It shows that in agreement with earlier observations [1], the cross-field transport becomes so fast at high densities that plasma flow into divertor cannot compete with it. Our findings support the hypothesis that the tokamak density limit (e. g. [24]) can be caused by cross-field plasma transport.

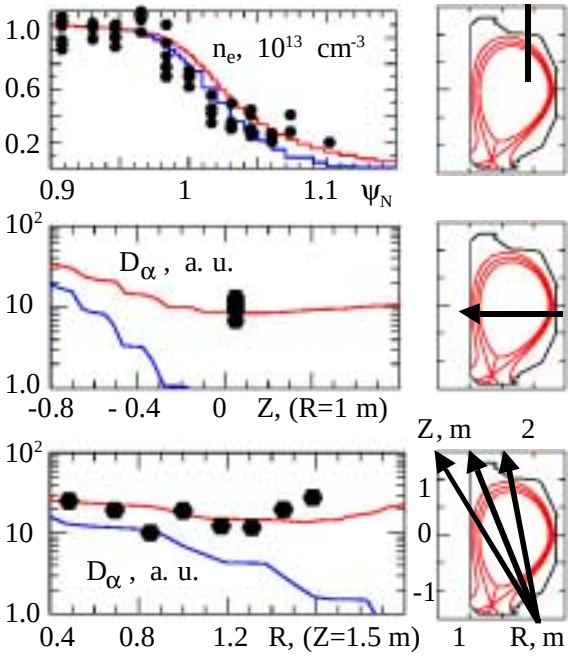

Fig. 6. Red (blue) curves represent modeling results with (without) convection. Dots are Thomson and Filterscope data.

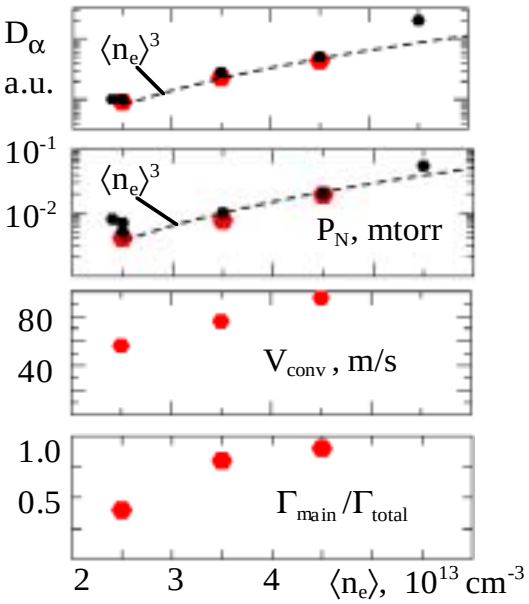

Fig. 7. Results of modeling of L mode plasmas having different $\langle n_e \rangle$. Red (black) dots represent our modeling (experiment).

What is also interesting is that both pure diffusive and diffusion/convection models are able to fit rather well few main parameters such as SOL plasma density and temperature profiles close to separatrix. However, the diffusive model fails to describe properly plasma transport in the far SOL with physically meaningful magnitude of diffusion coefficients in L mode and in between ELMs in H mode (see top panel in Fig. 6 and Fig. 8). The diffusive model finds much lower plasma flux to the wall, much lower neutral flux to the core, and much lower contribution of plasma convective energy loss to overall plasma energy balance than the hybrid diffusion/convection model.

As we pointed out before, fast cross-field plasma transport in the SOL affects not only mid plane plasma parameters, but also divertor ones. As an example, in Fig. 9 we show the results of our modeling of power load on the outer divertor target. As one sees fast cross field plasma transport in the SOL causes significant decrease of peak load in this radiative divertor shot. It implies that divertor detachment process can be strongly altered by blobby plasma transport in the SOL.

Conclusions. We demonstrate analytically that, due to ∇B polarization and effective sheath resistivity, plasma blobs in tokamak SOL can propagate radially with velocity ~ few km/s for distances ~10 cm and play a crucial role in edge cross field plasma transport.

Our 2D and 3D modeling support our analytic results and shows that blobs indeed are rather stable coherent structures which are able to move radially for large distances. Modeling of the dynamics of plasma dips indicates that they can be an important ingredient in impurity transport in the SOL and be responsible for a fast penetration of impurity ions to the core. To describe the effects of convective blobby transport on macroscopic edge plasma parameters we apply the plasma transport model which includes both diffusive and outward convective terms for cross-field plasma particle flux in the UEDGE code. We show that convective terms are crucially important to reproduce experimental data not only in the main chamber SOL region but in the divertor as well. Moreover, radial convection becomes the dominant plasma transport mechanism in the SOL at high plasma density.

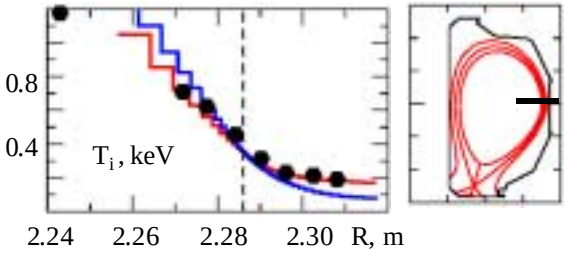

Fig. 8. Ion temperature in H mode edge plasma. Red (blue) curve diffusion/convection (diffusive) model. Dots are CHERS experimental points.

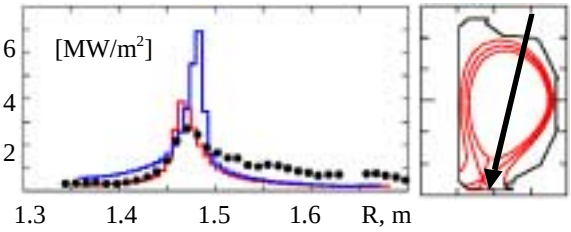

Fig. 9. Power loading on outer divertor plate. Red (blue) curve diffusion/convection (diffusive) model. Dots are IRTV experimental points

Acknowledgments. Supported by the US DoE.

References

[1] M. Umansky, et al., Phys. Plasma **5** (1998) 3373.
[2] R. Schneider et al, 17th IAEA, Japan, 19-24 October 1998, paper F1-CN-69/THP2/05.
[3] B. Lipschultz et al., 18th IAEA, Italy, 4-10 October 2000, paper IAEA-CN-77/EX5/6.
[4] S. I. Krasheninnikov, Phys. Letters A, **283** (2001) 368.
[5] R. Maqueda, Private communication, 1998.
[6] J. L. Terry, et al., J. Nuclear Material, **290-293** (2001) 757.
[7] J. A. Boedo, et al., Phys. Plasmas **8** (2001) 4826.
[8] D. L. Rudakov, et al., Plasma Phys. Control. Fusion **44** (2002) 717.
[9] J. Neuhauser, et al., Plasma Phys. Control. Fusion **44** (2002) 855.
[10] G. Y. Antar, et al., Phys. Rev. Lett. 87 (2001) 065001.
[11] H. W. Muller, et al., 29th EPS, O-2.06 (2002).
[12] S. J. Zweben, et al., Phys. Plasmas, **9** (2002) 1981.
[13] A. V. Nedospasov, et al., Nuclear Fusion **25** (1985) 21.
[14] Y. Sarazin and Ph. Ghendrih, Phys. Plasmas **5** (1998) 4214.
[15] S. I. Krasheninnikov, et al, 29th EPS, P3-205 (2002).
[16] D. A. D Ippolito, et al., Phys. Plasmas **9** (2002) 222.
[17] N. Biant, S. Benkadda, and J-V. Pausen, (2002) to be published.
[18] S. A. Galkin et al., Sherwood Conference 2002.
[19] J. A. Boedo, et al., 15th PSI, 2002.
[20] X. Q. Xu, et al., Nucl. Fusion **40** (2000) 731; **42** (2002) 2127.
[21] T. D. Rognlien et al., J. Nucl. Materials **196/198** (1992) 347.
[22] A. Yu. Pigarov, et al., Phys. Plasmas **9** (2002) 1287.
[23] A. Yu. Pigarov, et al., 15th PSI, 2002.
[24] M. Greenwald, Plasma Phys. Control. Fusion **44** (2002) R27–R80.